

# The influence of geometry, surface character and flexibility on the permeation of ions and water through biological pores

Oliver Beckstein and Mark S. P. Sansom\*

12th February 2004

Extended (ca. 0.1  $\mu$ s) molecular dynamics simulations are employed to test the hypothesis that a hydrophobic constriction site can act as an efficient barrier to ion and water permeation if its diameter is less than the diameter of an ion's first hydration shell. This hydrophobic gating mechanism is thought to operate in a number of ion channels, e.g. the nicotinic receptor, the bacterial mechanosensitive channels (MscL and MscS) and the potassium channels (KcsA, MthK, KvAP and KirBac). Simplified pore models allow one to investigate the primary characteristics of a conduction pathway, namely its geometry (shape, pore length and radius), the chemical character of the pore wall surface and its local flexibility and surface roughness. Our simulations show that a short hydrophobic pore is closed to water for radii smaller than 0.45 nm. By increasing the polarity of the pore wall (and thus reducing its hydrophobicity) the transition radius can be decreased until for hydrophilic pores liquid water is stable down to a radius comparable to a water molecule's radius. Ions behave similarly but the transition from conducting to non-conducting pores is even steeper and occurs at a radius of 0.65 nm for hydrophobic pores. The presence of water vapour in a constriction zone indicates a barrier for ion permeation. A thermodynamic model can explain the behaviour of water in nanopores in terms of the surface tensions, which leads to a simple measure of "hydrophobicity" in this context. Furthermore, increased local flexibility decreases the permeability of polar species. An increase in temperature has the same effect, and we hypothesise that both effects can be explained by a decrease of the effective solvent-surface attraction which in turn leads to an increase in the solvent-wall surface free energy.

---

\*Department of Biochemistry, University of Oxford, South Parks Road, Oxford OX1 3QU, UK. e-mail: oliver@biop.ox.ac.uk, WWW: <http://sansom.biop.ox.ac.uk/>

# 1 Introduction

Although only about 3 nm thick, the membranes of living cells present an efficient barrier to polar substances such as water or ions. Transport of water and ions into and out of the cell is facilitated by specialised proteins. For molecules that move down their electro-osmotic gradients the proteins are ion channels [1] and water pores (aquaporins) [2]. They share common functional characteristics such as high specificity (for instance, the potassium channel KcsA prefers potassium ions over sodium ions, aquaporins allow the flow of water but not of ions or protons) and transport rates comparable to diffusion in bulk solution. Ion channels can also be switched (“gated”) between an open (ion conducting) and closed (ion blocking) state by external signals such as changes in transmembrane voltage, binding of a ligand, mechanical stress etc.

In recent years a number of near atomic resolution structures of ion channels [3–12] and aquaporins [13–16] have been published. Based on these structures an atomistic understanding of the transport and gating properties is emerging. If we view transport proteins as molecular machines which are designed by evolution to perform selective and efficient transport that can be controlled, i.e. gated, then we can ask what the “building blocks” of these machines are. This involves not only identification and structural characterisation of the protein domains involved in gating, but also, at a more abstract level, understanding the underlying physical principles.

Here we address the questions of what are physical properties that are important for the permeation of ions and water, and what is their effect? In particular we will

focus on how the flow of ions and water can be controlled, i.e. we will investigate possible gating mechanisms. This interest is based on the observation that the putative gate in many known ion channel structures (in particular, the nicotinic acetylcholine receptor nAChR [12], the bacterial potassium channels KcsA [3] and KirBac1.1 [11], and the mechanosensitive channels MscL [4] and MscS [6]) is formed by a constriction made from hydrophobic residues. For example, the closed state nAChR structure displays an ion pathway which is still wide enough (radius  $R \approx 0.31$  nm) to admit three water molecules (radius of a water molecule  $r_w = 0.14$  nm) or one potassium ion ( $r_{K^+} = 0.133$  nm) with half of its first hydration shell intact. It is somewhat surprising that a pore does not have to be completely physically occluded to prevent the flow of ions. On the other hand ions can readily move through the KcsA [3, 5] selectivity filter although its radius is less than 0.15 nm. When an ion enters the filter it has to lose its hydration shell at a high cost in free energy—the solvation free energy for a potassium ion is about  $-320$  kJ mol $^{-1}$  [17]. The filter is lined by backbone oxygen atoms which coordinate the potassium ion and substitute for its hydration shell, thus reducing the desolvation barrier of  $+320$  kJ mol $^{-1}$  to about  $+12$  kJ mol $^{-1}$  [18]. The putative gates differ in that they are lined by hydrophobic residues. For nAChR [12, 19] and MscL [4, 20] it was already hypothesised that these residues cannot substitute for water molecules so that the energetic cost of desolvation prevents the passage of the ion.

It appears that the *geometry* of a pore (its radius, length and shape) and the *chemical character of the pore wall* have a great influence on the permeation of ions

and water. In addition, *local flexibility* (i.e. fluctuations in the protein structure as opposed to concerted larger scale motions) of the pore lining might play a role, as seen in simulations of  $K^+$  permeation through KcsA [18].

It seems difficult to comprehend the dynamical nature of transport phenomena from static crystal structures alone. Computational methods can be used to complement the experimentally observed picture. In particular, classical molecular dynamics (MD) can be used to investigate the behaviour of water or ionic solutions in the environment presented by a protein. This realistic environment, however, makes it difficult to disentangle the contributions of various pore properties. In order to be able to reduce the number of parameters simplified pore models can be designed to capture the characteristics in question [21–27]. We focus on the influence of geometry, pore wall character and flexibility. In previous studies we investigated the behaviour of water in these “nanopores”. In particular, we found that below a critical radius liquid water becomes unstable in the pore and the pore is predominantly filled with water vapour [27]. We hypothesised that a pore environment which cannot sustain liquid water would also present a high energetic barrier to an ion [23]. Although it seems plausible that absence of water would imply the absence of ions it has not been demonstrated previously.

In this work we explicitly consider ions in model pores and explore dimensions, pore wall character and flexibility in more detail than in our previous work. We also present a simple thermodynamic model based on surface energies that explains the observed behaviour of water in hydrophobic pores.

## 2 Methods and Theory

### 2.1 Model

The pore models were constructed as described previously [27]. Briefly, they consist of concentric rings of methane-like pseudo-atoms of van der Waals radius 0.195 nm (Figure 1). They are held in their equilibrium position by harmonic constraints with spring constant  $k_0 = 1000 \text{ kJ mol}^{-1} \text{ nm}^{-2}$ . They consist of two mouth regions (length 0.4 nm, i.e. one layer of pseudo atoms, and radius 1.0 nm) at either end of the constriction site of length  $L$  (varied between 0.4 nm and 2.0 nm) and radius  $R$  (varied between 0.15 nm and 1.0 nm). The pore was embedded in a membrane mimetic, a slab of pseudo atoms held on a cubic lattice with unit cell length 0.39 nm with harmonic springs of strength  $k_0$ . Pores with a polar surface were created by placing partial charges of  $\pm 0.38e$  on atomic sites 0.2 nm apart. The resulting dipole moments pointed parallel to the pore axis with a magnitude of 3.6 D, which is comparable to the dipole moment of the peptide bond (ca. 3.7 D [28]).

### 2.2 Molecular Dynamics

MD simulations were performed with GROMACS v3.1.4 [31] and the SPC water model [32]. The Lennard-Jones-parameters for the interaction between a methane-like pseudo-atom and the water oxygen are  $\epsilon_{CO} = 0.906493 \text{ kJ mol}^{-1}$  and  $\sigma_{CO} = 0.342692 \text{ nm}$ ; parameters for sodium and chloride ions are taken from the GROMACS force field. The integration time step was 2 fs and coordinates were saved every 2 ps. With periodic bound-

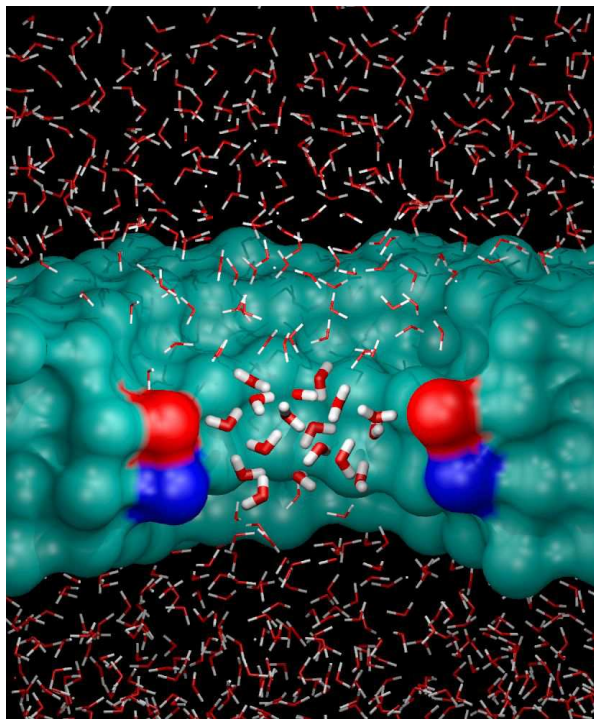


**Figure 1:** Simulation system: The solvent-accessible surface of a model pore with pore radius  $R = 0.55$  nm is shown in light blue (parts of the pore close to the observer are removed for clarity). The pore is not completely hydrophobic due to two dipoles (red/blue) in the pore wall which have the same magnitude as the peptide bond dipole. Water molecules in the pore are depicted in licorice representation and as lines in the mouth region or the bulk (image created with VMD [29] and Raster3D [30]).

ary conditions, long range electrostatic interactions were computed with a particle mesh Ewald method (real space cutoff 1 nm, grid spacing 0.15 nm, 4th order interpolation [33]) while the short range van der Waals forces were calculated within a radius of 1 nm. The neighbour list (radius 1 nm) was updated every 10 steps. Weak coupling algorithms [34] were used to simulate at constant temperature ( $T = 300$  K, time constant 0.1 ps) and pressure ( $P = 1$  bar, compressibility  $4.5 \times 10^{-5}$  bar $^{-1}$ , time constant 1 ps) with the  $x$  and  $y$  dimensions of the simulation cell held fixed at 4 nm. The total thickness of the water reservoir in the  $z$ -direction was 3.0 nm, en-

suring bulk-like water behaviour far from the membrane mimetic. A typical simulation box measured  $3.9 \times 3.9 \times 4.6$  nm $^3$  and contained about 1500 water molecules and 280 pseudo atoms.

### 2.3 State based analysis

We define discrete states by mapping equilibrium states of the whole system (snapshots from the MD equilibrium trajectory) onto numbers  $\omega_i$ . The same approach is used in statistical mechanics to map different microscopic states to one macroscopic state, characterised by the value of a state variable, here called  $\omega$ . The simplest example is a two-state system, e.g. liquid-

vapour: If water in the pore is liquid (density close to its bulk density) then  $\omega = 1$ , if it is vapour then  $\omega = 0$ .

Liquid-filled pores and vapour-filled pores are assumed to be in equilibrium. The openness (or probability for the occurrence of the liquid, i.e. open or water conducting state) is

$$\langle \omega \rangle = \frac{1}{T_{\text{sim}}} \int_0^{T_{\text{sim}}} dt \omega(t) = \frac{T_o}{T_{\text{sim}}}, \quad (1)$$

where  $T_{\text{sim}}$  denotes the total simulation time,  $T_o$  the total time that the pore is *open*, whereas  $T_c$  is the total time in the vapour or closed state. If  $\langle \omega \rangle > \frac{1}{2}$  then equilibrium is on the side of liquid (and vapour is a meta stable state), otherwise the stable state is vapour. The equilibrium is governed by the equilibrium constant

$$K(R) = \frac{T_c(R)}{T_o(R)} = \frac{T_{\text{sim}} - T_o(R)}{T_o(R)} \quad (2)$$

$$= \langle \omega(R) \rangle^{-1} - 1$$

which is trivially related to the openness.

## 2.4 Thermodynamic model for liquid-vapour equilibrium in pores

The equilibrium constant is determined by the free energy difference between the two

states. In the case of the model pores the grand potential  $\Omega(T, V, \mu) = -pV$  is the appropriate free energy [26]. At constant chemical potential  $\mu$  outside the pore (and with  $\beta^{-1} = k_B T$ )

$$\beta \Delta \Omega(R) = \beta [\Omega_c(R) - \Omega_o(R)] = -\ln K(R)$$

$$= -\ln(\langle \omega(R) \rangle^{-1} - 1) \quad (3)$$

holds. Following Evans [35], we write the free energy difference between the vapour and the liquid state with the corresponding surface contributions as

$$\Delta \Omega(R) = \Omega_v(R) - \Omega_l(R)$$

$$= -p_v(T, \mu) L \pi R^2 + 2\pi R L \gamma_{vw} + 2\pi R^2 \gamma_{lv}$$

$$- (-p_l(T, \mu) L \pi R^2 + 2\pi R L \gamma_{lw}) \quad (4)$$

The system is fairly close to bulk phase coexistence so we can expand the pressure around the saturation chemical potential  $\mu_{\text{sat}}(T)$  in a Taylor series

$$p(T, \mu) = p(T, \mu_{\text{sat}})$$

$$+ (\mu - \mu_{\text{sat}}) \left. \frac{\partial p(T, \mu)}{\partial \mu} \right|_{\mu=\mu_{\text{sat}}} + \dots, \quad (5)$$

where at saturation  $p_l(T, \mu_{\text{sat}}) = p_v(T, \mu_{\text{sat}})$ . This leads to a simple parabolic form for the free energy difference between the two states:

$$\Delta \Omega(R) = \left[ 2\gamma_{lv} - (\mu - \mu_{\text{sat}}) (n_v(T, \mu_{\text{sat}}) - n_l(T, \mu_{\text{sat}})) L \right] \pi R^2 + 2\pi L (\gamma_{vw} - \gamma_{lw}) R$$

$$= 2 \left[ \gamma_{lv} + \frac{1}{2} \Delta \mu \Delta n_{vl} L \right] \pi R^2 + 2\pi L \Delta \gamma_w R, \quad (6)$$

where we define the distance of the state from saturation  $\Delta \mu := \mu - \mu_{\text{sat}}$ , the difference in densities  $\Delta n_{vl} := n_l - n_v$  at sat-

uration, and the difference in surface free energies of the two phases with the wall,  $\Delta \gamma_w := \gamma_{vw} - \gamma_{lw}$ . The term  $\Delta \mu \Delta n_{vl} L$

is small for  $L < 10$  nm as the system is close to phase coexistence (for  $L \approx 1$  nm it is about  $10^{-3}$  times smaller than  $\gamma_{lv} = 17 k_B T \text{nm}^{-2}$  when estimated from  $\Delta n_{vl} \Delta \mu L \approx \Delta P L \approx 1 \text{ bar} \times L = 2.4 \times 10^{-3} k_B T \text{nm}^{-2} \times L$ ,  $T = 300$  K) and will be neglected. Only the difference between the surface free energies enters the model so we express it as the contact angle  $\theta_e$ , using the macroscopic definition from Young's equation  $\gamma_{vw} - \gamma_{lw} = \gamma_{lv} \cos \theta_e$  (see, for instance, Ref. [36]). Then Equation 6 becomes

$$\Delta\Omega(R, L, \theta_e) = 2\pi R \gamma_{lv} (R + L \cos \theta_e). \quad (7)$$

(Equation 7 is similar to the simple model derived by Allen et al. [26] but it includes  $\gamma_{vw} - \gamma_{lw}$  and hence  $\theta_e$  instead of just  $\gamma_{lv}$ .) For fixed pore length  $L$  and a given pore material, characterised by  $\theta_e$ , the graph of  $\Delta\Omega(R)$  over the pore radius  $R$  describes a parabola containing the origin. Although it is not *a priori* obvious that such a macroscopic treatment (Equation 6 or Equation 7) of a nanoscale system is meaningful the MD results for the free energy difference presented in Section 3.1 can be adequately explained within this model.

The connection between the model free energy  $\Delta\Omega(R)$  and the ‘‘functional’’ behaviour of the system as observed in MD simulations, i.e. the openness  $\langle \omega(R) \rangle$ , is established by inverting Equation 3,

$$\langle \omega(R) \rangle = \frac{1}{1 + \exp[-\beta \Delta\Omega(R)]}. \quad (8)$$

For linear  $\Delta\Omega(R)$  this represents a sigmoidal curve but non-linear terms (as in Equation 6) change its shape considerably.

### 3 Results and Discussion

First we investigate the behaviour of pure water in nanopores and quantify the influ-

ence of geometry, pore surface and local flexibility on the equilibrium between liquid and vapour filled pores. Then simulations for a NaCl electrolyte are analysed and compared to the pure water case. The intention behind these studies is to explore more fully the ways in which a hydrophobic gate may be opened, and how other factors might modulate such hydrophobic gating. This is particularly important in the context of current models for the gating of nAChR [12, 37] that suggest that the transition between the closed and open states of the pore involves both an increase in pore radius and in polarity. We also note that recent discussion of the state (open vs. closed) of MscS have suggested a hydrophobic gating mechanism [38], similar to that proposed for nAChR [23].

#### 3.1 Pure water

A large number of simulations were run for water in model pores (total simulation time  $> 5 \mu\text{s}$ ) in order to investigate the influence of pore radius ( $0.15 \text{ nm} \leq R \leq 1 \text{ nm}$ ) and pore surface character (hydrophobic vs. amphipathic vs. hydrophilic). Local flexibility (wall atom positional root mean square deviations (RMSDs)  $0.039 \text{ nm} \leq \rho \leq 0.192 \text{ nm}$ ) and temperature dependence in the range  $273 \text{ K} \leq T \leq 450 \text{ K}$  were examined for a hydrophobic  $R = 0.55 \text{ nm}$  pore.

#### Pore dimensions and surface character

The water density in short nanopores oscillates between liquid and vapour on a nanosecond time scale as seen in Figure 2, a manifestation of capillary evaporation at the nanoscale [27]. In Figure 3 the openness and the free energy difference  $\Delta\Omega$  between vapour and liquid states is shown

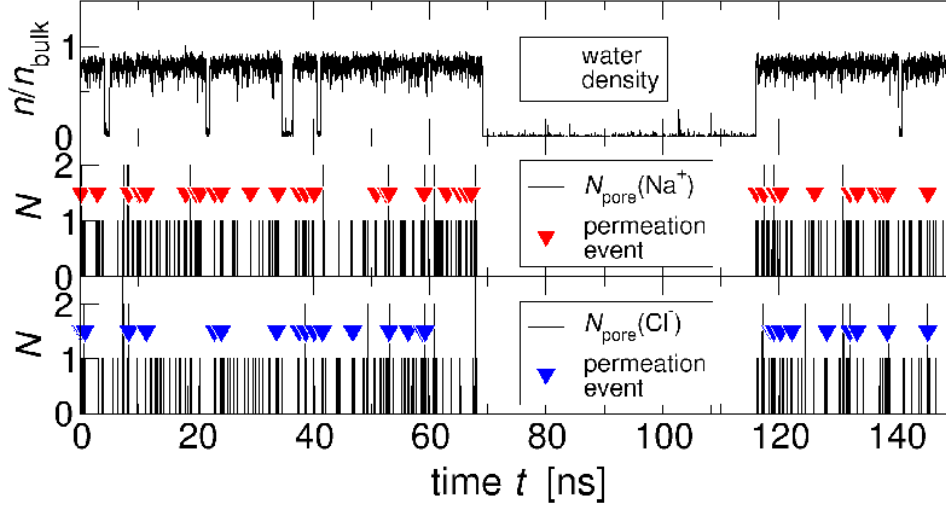


**Figure 2:** Liquid-vapour oscillations of water in a  $R = 0.65$  nm apolar pore (top panel) when bathed in a 1.3 M NaCl solution. As indicated by the number  $N$  of ions within the pore, sodium (middle) and chloride ions (bottom) are only observed in the pore when there is also liquid water ( $n/n_{\text{bulk}} \approx 0.8$ ) present. Permeation events are indicated by triangles; ions do not permeate the pore during the vapour phases.

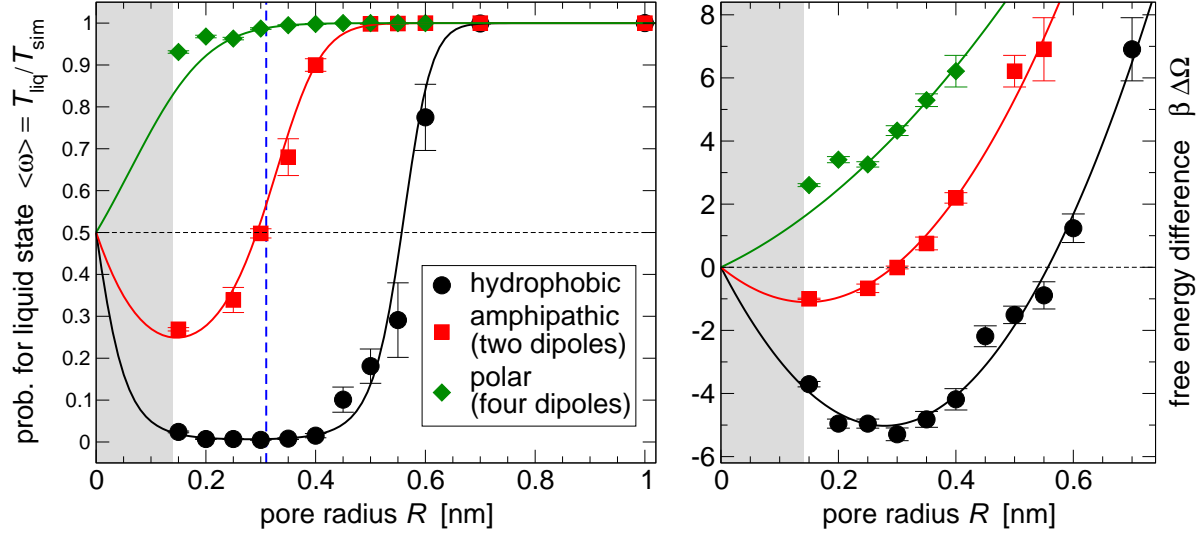


**Figure 3:** Water in model pores. Left: openness  $\langle \omega \rangle$  over radius. Right: free energy difference  $\Delta \Omega$  (in  $k_B T$ ) between vapour and liquid state. The grey region indicates radii smaller than the radius of a water molecule (0.14 nm). Data points are obtained from MD simulations with the errors estimated from block averages [41]. The continuous lines are fits of the model (Equation 6) to the data points (right) or the openness computed from the model (Equation 8). The vertical line indicates the radius of the closed nAChR gate ( $R = 0.31$  nm).

**Table 1:** Parameters of the thermodynamic model Equation 6 fitted to the MD results and resulting contact angle  $\theta_e$ . Experimental values for  $\gamma_{lv} = 72 \times 10^{-3} \text{ Jm}^{-2} = 17 k_B T \text{ nm}^{-2}$  and  $\theta_e \approx 118^\circ$  for water on a flat methyl ( $-\text{CH}_3$ ) terminated self assembled monolayer [39, 40] indicate that the simple thermodynamic model gives the right order of magnitude results. (All values at room temperature)

pore surface character			$\gamma_{lv} + \frac{1}{2}\Delta\mu \Delta n_{vl} L$ [ $k_B T \text{ nm}^{-2}$ ]	$\Delta\gamma_w = \gamma_{vw} - \gamma_{lw}$ [ $k_B T \text{ nm}^{-2}$ ]	$\theta_e$ [ $^\circ$ ]
bare $\text{CH}_4$	$0$	“hydrophobic”	$+11 \pm 1$	$-7.2 \pm 0.2$	$131 \pm 5$
two dipoles	$D2$	“amphipathic”	$+8.2 \pm 0.5$	$-3.0 \pm 0.0$	$111 \pm 1$
four dipoles	$D4$	“hydrophilic”	$+2.9 \pm 0.5$	$+1.8 \pm 0.2$	$52 \pm 9$

for different pore surfaces. For hydrophobic and amphipathic pores a strong dependence of the pore state on the radius is apparent. The stable thermodynamic state switches from vapour ( $\Delta\Omega < 0$  or  $\langle\omega\rangle < \frac{1}{2}$ ) to liquid ( $\Delta\Omega > 0$  or  $\langle\omega\rangle > \frac{1}{2}$ ) at a critical radius  $R_c$ , which is 0.57 nm for the hydrophobic pore and 0.3 nm for the amphipathic one. The functional form Equation 6 fits the data from the MD simulations (Table 1) well (the continuous lines in Figure 3). The coefficient of the quadratic term,  $\gamma_{lv} + \frac{1}{2}\Delta\mu \Delta n_{vl} L$ , is positive and similar for both the hydrophobic and the amphipathic (two dipoles, abbreviated  $D2$ ) pores (Table 1), consistent with the model Equation 6, which predicts this coefficient to be independent of the pore wall. For the polar pore (four dipoles,  $D4$ ) it is positive (but about three times smaller) only when the first two data points are ignored as outliers (possibly due to the strong influence of the dipole ends on the bulk-like water in the vicinity of the narrow pore entrance). The coefficient is in fact dominated by the water liquid-vapour surface tension  $\gamma_{lv}$  (see Section 2.4) and hence we will use its value for  $\gamma_{lv}$ .  $\Delta\gamma_w$ , the difference in surface tensions between the wall and vapour or liquid, becomes more positive with in-

creasing polarity of the pore wall. It effectively measures the hydrophobicity of the wall. This becomes even more apparent when the (macroscopic) contact angle  $\cos\theta_e = \Delta\gamma_w/\gamma_{lv}$  is formally computed (Table 1). Macroscopically, a hydrophobic surface can be defined as one with  $\theta_e > 90^\circ$ . This allows us to call the apolar pore ( $\theta_e = 131^\circ$ ) “hydrophobic” compared to the “amphipathic” pore  $D2$  ( $\theta_e = 111^\circ$ ; still hydrophobic but with some “hydrophilic” patches). A “hydrophilic” pore like the  $D4$  system ( $\theta_e \approx 52^\circ$ ) is characterised by  $\Delta\gamma_w > 0$  or  $\theta_e < 90^\circ$  and liquid is always the preferred phase in the pore, regardless of  $R$ .

Experimental macroscopic contact angles  $\theta_e$  for water on flat methyl ( $-\text{CH}_3$ ) terminated self assembled monolayers are reported up to  $118^\circ$  [39, 40]. A “microscopic contact angle” of  $135^\circ \pm 15^\circ$  was calculated for a droplet of 90 water molecules (radius  $R \approx 0.75$  nm) on a methyl terminated film from MD simulations [42], consistent with our result of  $\theta_e = 131^\circ$ . MD simulations seem to overestimate the experimental equilibrium contact angle. In this context we note that although the macroscopic equilibrium contact angle is only established about 10 nm from the contact

line, the local contact angle  $\theta_l$  in the core structure of the contact line (in the region 3–10 nm from the contact line) in water (and electrolytes) is predicted to be *larger* than  $\theta_e$  due to electrostatic screening effects [36].

From the model free energy the openness can be calculated (Equation 8) and displayed together with the MD results (Figure 3). Because the model effectively treats the liquid as a structureless continuum it is not meaningful to extrapolate to radii smaller than the radius of a water molecule (the shaded region in Figure 3). Nevertheless, the MD results lie on the model curve even in the direct vicinity of this region. Further tests of Equation 7 by varying the length of the pore together with the radius confirm the model qualitatively (data not shown).

Our model implies that for both nano- and mesoscale pores the cost of creating the liquid-vapour interface is the only force driving the filling of a hydrophobic ( $\Delta\gamma_w \leq 0$ ) pore; the gain in free energy by creating a bulk-like liquid compared to vapour in the pore is negligible.

**Local flexibility** The influence of local fluctuations in protein structure can be modelled by changing the harmonic spring constant  $k$  that holds the pore wall atoms at their equilibrium positions. In a simplified picture of a harmonic oscillator with an average energy  $k_B T/2$  per degree of freedom the RMSD  $\rho$  is directly related to  $k$  by  $\rho(k) = \sqrt{\langle \Delta r_{\max} \rangle^2} = \sqrt{3k_B T/k}$ . This simple model overestimates the measured RMSDs by only 10–20% (Table 2), showing that the wall atoms behave like almost independent, thermally driven, harmonic oscillators (Figure 4a). At a fixed radius, increasing the flexibility (smaller

$k$ , hence greater  $\rho$ ) shifts the equilibrium towards vapour (Figure 4). Conversely, a more rigid wall favours the condensation of water in the pore. Thus, water does not “push away” the pore walls to fill the pore but rather fluctuating pore walls appear to disfavour the formation of adjacent water layers. This effect cannot be explained with the assumption that the water molecules encounter a more narrow pore “on average”. Even if one assumes that the pore is narrowed by the RMSD of an atom down to an effective radius  $R(k) = R_0 - \rho(k)$ , the effect is still much stronger. When the thermodynamic model and the parameters for the hydrophobic pore (from Table 1 where  $k_0 = 4 \times 10^2 k_B T \text{ nm}^{-2}$ ) are used to predict  $\Delta\Omega(R(k))$  then the prediction compared to the simulation results underestimates the effect for the more flexible pores but is in agreement for more rigid pores (Figure 4b). We hypothesise that the random positional fluctuations of the wall atoms change the effective potential between the wall atom and water molecules by “smearing out” the attractive well of the interaction potential. Preliminary calculations showed that an increase in flexibility (or temperature) would always decrease the well depth of the Lennard-Jones potential, which is used to describe the interaction between a water molecule and the methane molecules of the pore wall. Nijmeijer et al. [43] demonstrated the dependence of the surface tension on the well depth  $\epsilon$  of the interaction potential analytically. MD simulations of a water droplet with 1000 molecules ( $R \approx 2.5 \text{ nm}$ ) on a graphite-like surface with varying well depth  $\epsilon_{\text{C-OW}}$  yielded a contact angle that varied from  $30^\circ$  to  $180^\circ$  [44]. Thus it is the well depth of the interaction potential which ultimately determines the

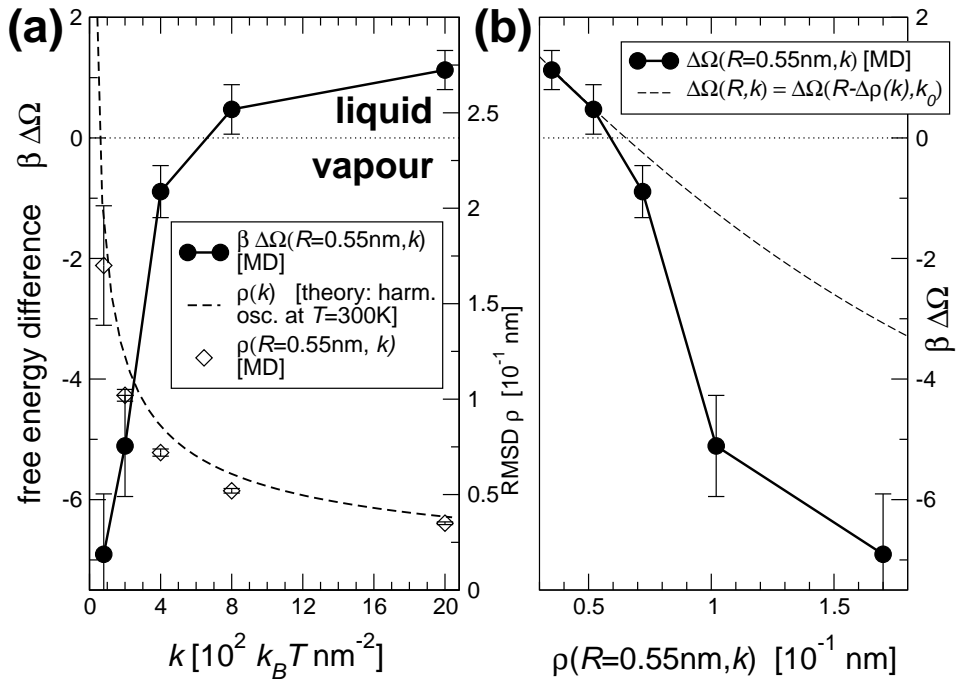


**Figure 4:** Influence of flexibility on the liquid-vapour equilibrium. (a) For a hydrophobic  $R = 0.55$  nm pore the harmonic restraint force constant  $k$  of the pore wall atoms was varied, resulting in a range of RMSDs  $\rho$ , which show the expected behaviour of thermal harmonic oscillators. The free energy difference  $\Delta \Omega$  between liquid and vapour states of water in the pore shows strong dependence on the local flexibility  $\rho$ ; rigid pores contain liquid water whereas flexible ones favour vapour. The effect can not be explained by a reduction of the effective pore radius by  $\rho$  alone [broken line in (b)]. All data at  $T = 300$  K.

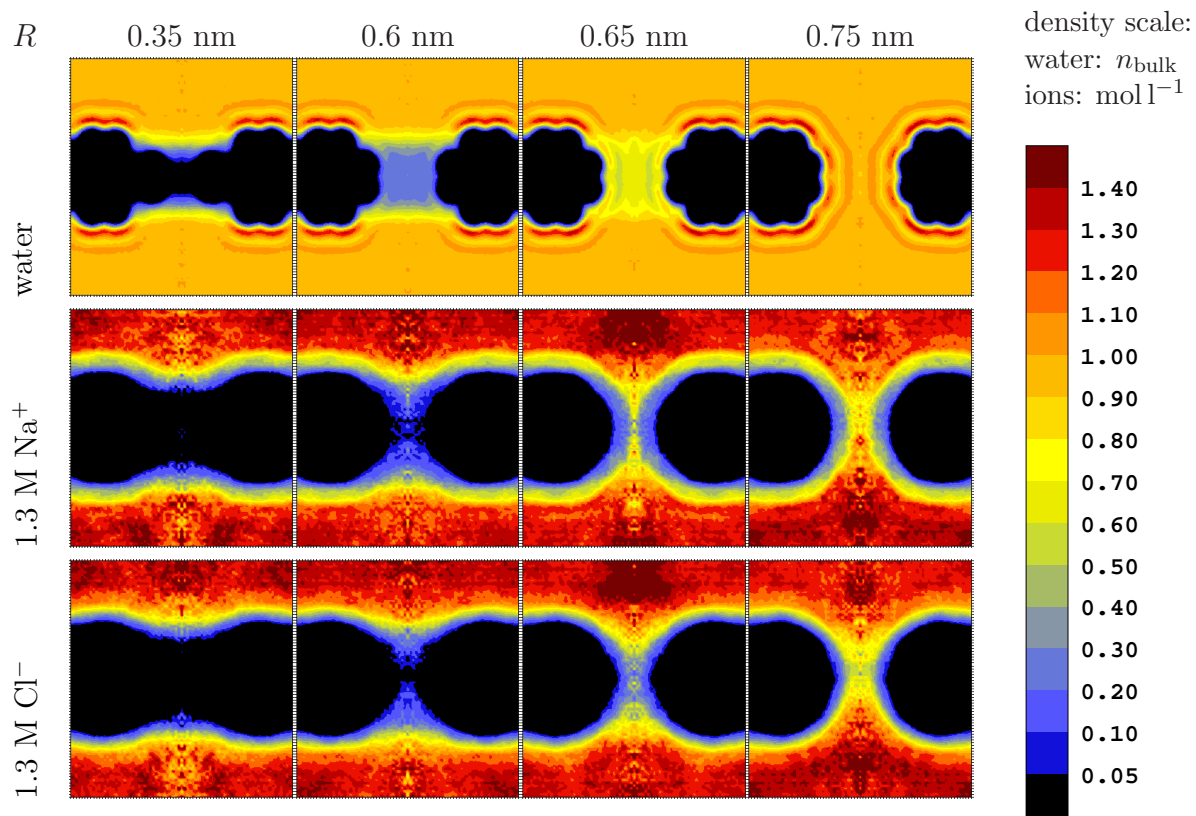
thermodynamic equilibrium in the pore. This is made explicit by considering Equation 6 and noting that  $\Delta \Omega(R)$  depends on the water-wall surface tensions through  $\gamma_{vw} - \gamma_{lw}$ , which in turn depend on  $\epsilon$ . For the case of water in confined geometries it was shown that capillary condensation and evaporation phenomena depend sensitively on  $\epsilon$  [27, 45, 46] (or more precisely, on the effective well depth, the product of the wall atom density with  $\epsilon$  [27]).

### 3.2 NaCl electrolyte

As mentioned in the Introduction it has been hypothesised that a local hydrophobic environment would present a signifi-

cant desolvation barrier to ion permeation. Our simulations of model pores bathed in a 1.3 M NaCl solution exhibit a striking change in the behaviour of the ions for pore radii  $R \geq 0.65$  nm. Figure 5 shows that in pores of comparable dimensions to the closed nAChR pore ( $R = 0.35$  nm) ions have a vanishing probability of entering the pore but at the open-state radius  $R = 0.65$  nm the pore density rises to half the bulk value. The average density of ions in the centre of the pore (Figure 6) exhibits a sharp increase near  $R = 0.65$  nm, similar to the behaviour of the openness (Figure 3).

The radially averaged densities show



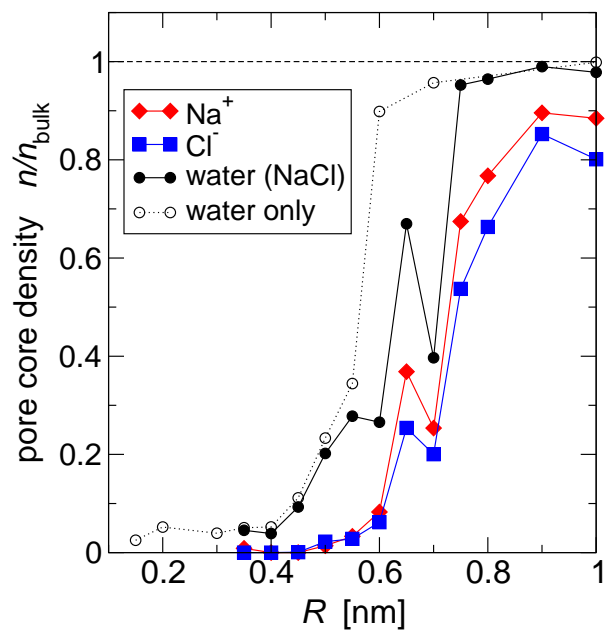


**Figure 6:** Ionic density in the core region of hydrophobic pores. The core is taken to have a radius of about one ionic radius (0.1 nm) and exhibits the highest density of ions. The core density increases markedly at the critical radius  $R = 0.65$  nm. The core density follows the openness (as shown for water in Figure 3). Bulk concentration of ions is 1.3 M. Lines are drawn as guides to the eye.

**Table 2:** RMSD of wall atoms in flexible pore models of radius  $R = 0.55$  nm and influence on the liquid-vapour equilibrium of water in the pore at  $T = 300$  K.

restraint force constant $k$ [ $10^2 \times k_B T \text{ nm}^{-2}$ ]	RMSD $\rho(k)$ [10 <sup>-1</sup> nm] MD	theory	$\langle \omega \rangle$ MD	$\beta \Delta \Omega$ MD
0.8	1.7±0.3	1.92	0.001±0.001	-6.9±1.0
2	1.0±0.0	1.22	0.006±0.005	-5.1±0.8
4	0.72±0.02	0.86	0.291±0.089	-0.89±0.43
8	0.52±0.01	0.61	0.616±0.097	0.47±0.41
20	0.35±0.01	0.39	0.755±0.060	1.1±0.3

two pronounced water layers with an inter-layer distance  $d = 0.3$  nm near the membrane mimetic. The ionic density drops off sharply at the maximum of the outermost water layer and vanishes completely at the maximum of the water layer closest to the surface. Sodium and chloride ions are both present at the same distance from the surface. Because the membrane mimetic carries no charge and represents a low dielectric region (as do the less mobile bound water layers) it is energetically more favourable for the ions to be solvated in the high dielectric region of the bulk-like water; furthermore, it would cost free energy to disturb the stable water layers. The bound water layers are not a consequence of the presence of the ions as they also form in pure water near a hydrophobic surface with the same inter-layer spacing of 0.3 nm [27], and in this case even a third water layer is discernible with  $d = 0.35$  nm. The third layer is probably not stable enough to withstand the pressure exerted by the ions in solution outside the second layer. Effectively, ions are excluded from a zone of thickness 0.6 nm ( $\text{Na}^+$ ) or 0.7 nm ( $\text{Cl}^-$ ) from the surface. The ion exclusion zone stretches into the pore without interruption so that at  $R = 0.65$  nm there is only a narrow

channel of easily displaceable water which can admit ions. For wider pores, the ion density in the pore approaches bulk values (Figure 6). This suggests that in addition to the cost of desolvation there is the additional cost of disturbing water layers which can prevent ions from permeating hydrophobic pores.

Although the absence of ionic density can be taken as a strong indication for a closed pore the presence of equilibrium density does not necessarily imply a functionally open state, as the latter also requires rapid permeation of ions through a pore. As MD simulations output the trajectories of water and ions, the equilibrium flux ( $\Phi_0$ ), i.e. the total number of particles per nanosecond which completely permeate the pore, can be measured. Figure 7 shows  $\Phi_0$  for ions and water molecules (both for water in a 1.3 M NaCl electrolyte and for pure water) in hydrophobic pores of varying radius on a logarithmic scale. Water flux is about three orders of magnitude larger than ion flux and increases rapidly with increasing smaller radii but beyond the critical radius  $R_c = 0.57$  nm (when liquid becomes the stable phase) the slope in the logarithmic plot decreases from 15 nm<sup>-1</sup> to 2.4 nm<sup>-1</sup>. The water current density  $\Phi_0/(\pi R^2)$  reaches a constant

value of  $300 \text{ ns}^{-1} \text{ nm}^{-2}$  so the increase for  $R > R_c$  is only due to the increase in pore diameter. The increase for  $R < R_c$  correlates with the openness (Figure 3), indicating that the main contribution to the flux stems from the open-state periods [27]. The presence of ions shifts  $R_c$  from ca. 0.6 nm for pure water to 0.75 nm for 1.3 M NaCl electrolyte. The reasons for this shift are not clear.

The total number of ions that successfully permeate the pore per nanosecond shows an increase over almost two orders of magnitude when the pore radius  $R$  is increased from 0.6 nm to 0.65 nm. Thus the pore “opens” at a radius much larger than the bare ionic radius. Ions permeate only when the pore is filled with liquid water (typical data in Figure 2) and  $\text{Na}^+$  permeation events are not correlated with  $\text{Cl}^-$  ions passing through the pore.

Because the simulations are in thermodynamic equilibrium the net flux through the pore is zero for all  $R$ . In order to compare the MD equilibrium flux  $\Phi_0$ , which is determined by the intrinsic barrier to ion permeation, to experimentally measured non-equilibrium fluxes  $\Phi$  of ions of charge  $q$  at a driving transmembrane voltage  $V$  we employ rate theory and estimate

$$\Phi(V; R) = \Phi_0(R) \sinh \frac{qV}{2k_B T}. \quad (9)$$

For  $R = 0.65 \text{ nm}$ ,  $V = 100 \text{ mV}$ ,  $q = 1e$  and  $T = 300 \text{ K}$  we obtain  $\Phi \approx 1.2 \text{ ns}^{-1}$ , which is 40 times larger than the experimental value of  $0.03 \text{ ns}^{-1}$  for nAChR at 0.2 M ionic concentration (calculated from a conductance of ca. 45 pS [1]). The discrepancy between our estimate and the experimental data is not unexpected as Equation 9 has only qualitative character. Furthermore, nAChR presents a more complex pore lining surface than the model

pore, and if the difference in bath concentrations and access resistance were taken into account the discrepancy would likely be reduced by an order of magnitude. Nevertheless, the estimate demonstrates that the intrinsic barrier to ion permeation is small beyond the critical radius.

### 3.3 Sensing external parameters

In the simplest model of sensing a system exists in an equilibrium with two states. External stimuli shift the equilibrium which elicits a cellular response. For example, a temperature-sensing channel at normal temperature might be in the closed state. Elevated temperature shifts the equilibrium to the open state and the influx of ions initiates a signalling cascade that terminates in the sensation of heat. However, the exact mechanisms of gating by temperature of e.g. TRP channels remain obscure [47]. We tested the influence of temperature in the range from 273 K to 450 K on water in the  $R = 0.55 \text{ nm}$  hydrophobic pore (data points for  $T > 373 \text{ K}$  represent “supercritical” water, as the SPC water model does not show a phase transition at the boiling point but remains liquid). The free energy landscape of the water-pore system depends on the temperature (Figure 8a). With increasing temperature the liquid state (i.e. near water bulk density) decreases in stability. Accordingly, the openness decreases with temperature so that the vapour state, i.e. the closed state, dominates at higher temperatures (Figure 8b). The decrease in openness with increasing  $T$  indicates that the difference of the wall surface tensions  $\Delta\gamma_w$  must become even more negative, i.e. vapour in contact with the wall is increasingly favoured. The effect would be similar to the one discussed for increased

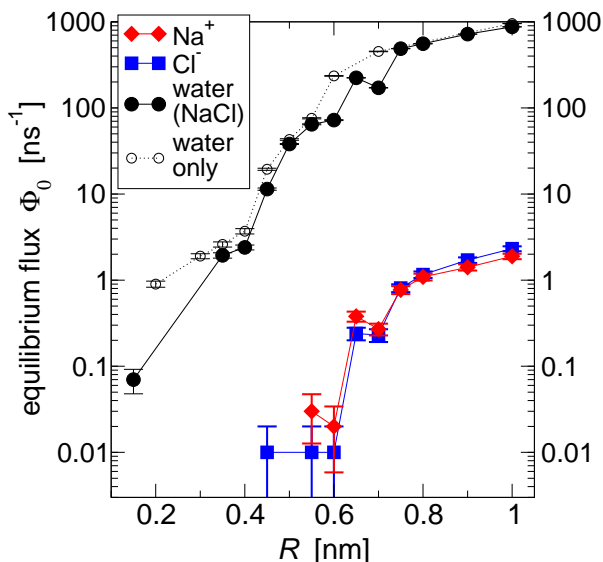


**Figure 7:** Equilibrium flux  $\Phi_0$  of water and ions through hydrophobic model pores. The total number of ions that successfully permeate the pore per nanosecond shows an increase over almost two orders of magnitude when the pore radius  $R$  is increased from 0.6 nm to 0.65 nm. Water flux increases with the radius and is not significantly influenced by the presence of 1.3 M NaCl except for the shift in the transition radius from 0.6 nm (only water) to 0.75 nm (water with NaCl). Lines are drawn to guide the eye and errors are estimated from block averages [41].

flexibility of wall atoms as the major effect of temperature would be to smear out the interaction potential between water molecules and wall atoms. This example demonstrates in principle how an external signal, an increase in temperature from  $T = 300$  K to 330 K, decreases the openness, and correspondingly the flux of water molecules, by a factor of 6.

## 4 Conclusions and outlook

We have explicitly demonstrated a hydrophobic gating mechanism for ions, using simplified hydrophobic pores as models for the closed gates of ion channels. There is a critical radius  $R_c$  above which a pore becomes effectively permeable to water or ions.  $R_c \approx 0.57$  nm for water and

$R_c \approx 0.65$  nm for ions, is much larger than the radius for a water molecule or a bare ion alone. This correlates nicely with the current view that the closed state structures of many ion channels contain gates formed by hydrophobic constriction sites. In nAChR the radius of the putative gate is 0.31 nm, 0.17 nm in MscL, and 0.13 nm in KcsA. Models of KcsA and of Kv channels in their open states, based on the MthK and KvAP structures respectively, have a gate radii of about 0.6 nm [48], whereas the open-state nAChR structure opens up to about 0.65 nm. Our simulations show that the polarity of the pore wall can shift the critical radius considerably. This is reflected in the proposed gating mechanism of nAChR [37]. Not only does the radius of the constriction site increase but hydrophobic sidechains are also

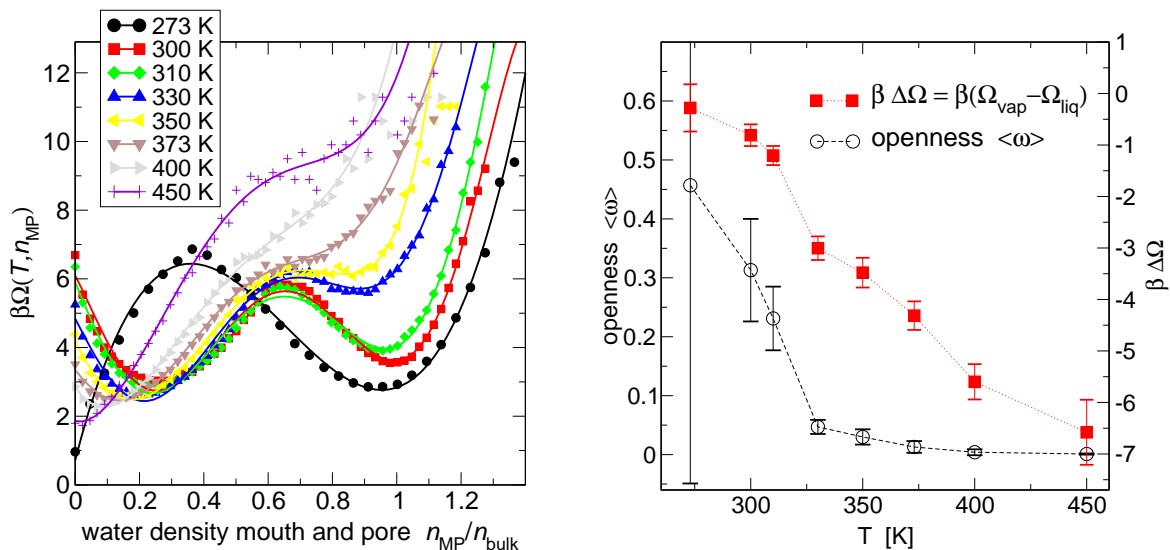


**Figure 8:** Temperature dependence of the liquid-vapour equilibrium in a hydrophobic  $R = 0.55$  nm pore. *Left:* Change of the free energy landscape  $\Omega(n, T)$  with  $T$ . The density is calculated over the pore and the mouth regions which act as a buffer of constant chemical potential, except for  $T = 273$  K, where the mouth region also fills with vapour. Continuous lines are polynomial least square fits of order 4 (or order 6 for  $300 \text{ K} \leq T \leq 330 \text{ K}$ ), reminiscent of a Landau free energy with the water density in the pore and mouth region  $n_{MP}$  as order parameter. *Right:* Openness and free energy difference between states  $\Delta\Omega$ .

rotated out of the pore to expose the more polar, i.e. hydrophilic, peptide backbone. By combining hydrophobic gating with a change in surface polarity only a moderate change in radius is required to obtain a large physiological effect. Changes in local flexibility may also modulate the gating behaviour. It is too early to ascertain their importance as they have not been widely investigated experimentally for channels (or any other proteins). There are some suggestions of possible regulatory roles of changes in flexibility in e.g. KTN domains [49] and in the modulation of binding of TRAP protein to the trp operon mRNA [50]. Temperature can also affect gating, in a fashion similar to local flexibility, but its direct effects seem too small to explain, for instance, the temperature sensitivity of TRP channels on their own.

A thermodynamic model based on surface energies fits remarkably well the data of the atomic-scale MD simulation, even for very small radii. Though such a macroscopic treatment is not *a priori* expected to give a satisfactory description of a microscopic system there are other examples as for instance classical nucleation theory, which shares some similarities with our and others' models [26, 51]. It generally agrees quite well with experiments on the condensation of droplets from vapour, which implies that the use of macroscopic surface tension is valid even for droplets of radii of about 1 nm [52]. It appears that in this case water structure (i.e. a hydrogen bond network) is only important insofar that it is responsible for different wall-fluid surface tensions. Our results seem to corroborate the conclusions of Maibaum and

Chandler [53] that two-state behaviour of water in pores should only require a cold liquid close to phase coexistence and sufficiently different vapour-wall and liquid-wall surface tensions.

We have sketched out principles of gating mechanisms in ion channels, based on model channels. Ion channels in nature display complex conformational dynamics in relationship to gating. There is a need for better single molecule methods for ion channels to probe these phenomena experimentally. Combined electrical and op-

tical methods look promising in this respect [54] although considerable improvements in time resolution are still required. In the meantime there is a continued role for simulations and theory to enable us to bridge between static structure and dynamic function.

**Acknowledgements** We are grateful for discussions with Paul Barrett, Kaihsu Tai, Campbell Millar, José Faraldo-Gómez, Benoît Roux and Nigel Unwin. This work was funded by The Wellcome Trust.

## Abbreviations list

**MD** molecular dynamics

**SPC** simple point charge water model

**RMSD** root mean square deviation

**nAChR** nicotinic acetylcholine receptor

**MscS** mechanosensitive channel of small conductance (*Escherichia coli*)

**MscL** mechanosensitive channel of large conductance (*Mycobacterium tuberculosis*)

**KcsA** potassium channel (*Streptomyces lividans*)

**KirBac1.1** inward rectifier potassium channel (*Burkholderia pseudomallei*)

**MthK** calcium-gated potassium channel (*Methanobacterium thermoautotrophicum*)

**KvAP** voltage-dependent potassium channel (*Aeropyrum pernix*)

**D2** model pore containing two dipoles (amphipathic)

**D4** model pore containing four dipoles (hydrophilic)

**TRP** transient receptor potential channel family

**KTN** potassium transport, nucleotide binding domain

**TRAP** trp RNA-binding attenuation protein

**trp** tryptophan

**mRNA** messenger RNA

## References

- [1] Hille B, 2001 *Ion Channels of Excitable Membranes*, 3rd edn. (Sinauer Associates, Sunderland MA, U.S.A.)
- [2] Fujiyoshi Y, Mitsuoka K, de Groot B L, Philippsen A, Grubmüller H, Agre P and Engel A, 2002 Structure and function of water channels. *Curr. Opin. Struct. Biol.* **12** 509–515
- [3] Doyle D A, Morais-Cabral J, Pfützner R A, Kuo A, Gulbis J M, Cohen S L, Chait B T and MacKinnon R, 1998 The structure of the potassium channel: molecular basis of K<sup>+</sup> conduction and selectivity. *Science* **280** 69–77
- [4] Chang G, Spencer R H, Lee A T, Barclay M T and Rees D C, 1998 Structure of the MscL

- homolog from *mycobacterium tuberculosis*: a gated mechanosensitive ion channel. *Science* **282** 2220–2226
- [5] Zhou Y, Morais-Cabral J H, Kaufman A and MacKinnon R, 2001 Chemistry of ion coordination and hydration revealed by a  $K^+$  channel-Fab complex at 2.0 Å resolution. *Nature* **414** 43–48
- [6] Bass R B, Strop P, Barclay M and Rees D C, 2002 Crystal structure of *escherichia coli* MscS, a voltage-modulated and mechanosensitive channel. *Science* **298** 1582–1587
- [7] Dutzler R, Campbell E B, Cadene M, Chait B T and MacKinnon R, 2002 X-ray structure of a ClC chloride channel at 3.0 Å reveals the molecular basis of anion selectivity. *Nature* **415** 287–294
- [8] Fujiyoshi Y, Mitsuoka K, de Groot B L, Philippsen A, Grubmüller H, Agre P and Engel A, 2002 Structure and function of water channels. *Curr. Opin. Struct. Biol.* **12** 509–15
- [9] Jiang Y, Lee A, Chen J, Cadene M, Chait B T and MacKinnon R, 2002 Crystal structure and mechanism of a calcium-gated potassium channel. *Nature* **417** 515–22
- [10] Jiang Y, Lee A, Chen J, Ruta V, Cadene M, Chait B T and MacKinnon R, 2003 X-ray structure of a voltage-dependent  $K^+$  channel. *Nature* **423** 33–41
- [11] Kuo A, Gulbis J M, Antcliff J F, Rahman T, Lowe E D, Zimmer J, Cuthbertson J, Ashcroft F M, Ezaki T and Doyle D A, 2003 Crystal structure of the potassium channel KirBac1.1 in the closed state. *Science* **300** 1922–1926
- [12] Miyazawa A, Fujiyoshi Y and Unwin N, 2003 Structure and gating mechanism of the acetylcholine receptor pore. *Nature* **423** 949–955
- [13] Murata K, Mitsuoka K, Hirai T, Walz T, Agre P, Heymann J B, Engel A and Fujiyoshi Y, 2000 Structural determinants of water permeation through aquaporin-1. *Nature* **407** 599–605
- [14] Fu D, Libson A, Miercke L J, Weitzman C, Nollert P, Krucinski J and Stroud R M, 2000 Structure of a glycerol-conducting channel and the basis for its selectivity. *Science* **290** 481–486
- [15] Sui H, Han B G, Lee J K, Walian P and Jap B K, 2001 Structural basis of water-specific transport through the AQP1 water channel. *Nature* **414** 872–878
- [16] Savage D F, Egea P F, Robles-Colmenares Y, III J D O and Stroud R M, 2003 Architecture and selectivity in aquaporins: 2.5 Å X-ray structure of aquaporin Z. *PLoS Biology* **1** 334–340
- [17] Lyubartsev A P, Førrisdahl O K and Laaksonen A, 1998 Solvation free energies of methane and alkali halide ion pairs: An expanded ensemble molecular dynamics simulation study. *J. Chem. Phys.* **108** 227–233
- [18] Bernèche S and Roux B, 2001 Energetics of ion conduction through the  $K^+$  channel. *Nature* **414** 73–77

- [19] Unwin N, 1993 Nicotinic acetylcholine-receptor at 9 Å resolution. *J. Mol. Biol.* **229** 1101–1124
- [20] Moe P C, Levin G and Blount P, 2000 Correlating a protein structure with function of a bacterial mechanosensitive channel. *J. Biol. Chem.* **275** 31121–31127
- [21] Lynden-Bell R M and Rasaiah J C, 1996 Mobility and solvation of ions in channels. *J. Chem. Phys.* **105** 9266–9280
- [22] Allen T W, Kuyucak S and Chung S H, 1999 The effect of hydrophobic and hydrophilic channel walls on the structure and diffusion of water and ions. *J. Chem. Phys.* **111** 7985–7999
- [23] Beckstein O, Biggin P C and Sansom M S P, 2001 A hydrophobic gating mechanism for nanopores. *J. Phys. Chem. B* **105** 12902–12905
- [24] Crozier P S, Henderson D, Rowley R L and Busath D D, 2001 Model channel ion currents in NaCl-Extended Simple Point Charge water solution with applied-field molecular dynamics. *Biophys. J.* **81** 3077–3089
- [25] Allen R, Melchionna S and Hansen J P, 2002 Intermittent permeation of cylindrical nanopores by water. *Phys. Rev. Lett.* **89** 175502–1–175502–4
- [26] Allen R, Hansen J P and Melchionna S, 2003 Molecular dynamics investigation of water permeation through nanopores. *J. Chem. Phys.* **119** 3905–3919
- [27] Beckstein O and Sansom M S P, 2003 Liquid-vapor oscillations of water in hydrophobic nanopores. *Proc. Natl. Acad. Sci. USA* **100** 7063–7068
- [28] Eisenberg D and Crothers D, 1979 *Physical Chemistry with Applications to the Life Sciences* (The Benjamin/Cummings Publishing Company, Menlo Park, California)
- [29] Humphrey W, Dalke A and Schulten K, 1996 VMD – Visual Molecular Dynamics. *J. Mol. Graph.* **14** 33–38, URL <http://www.ks.uiuc.edu/Research/vmd/>
- [30] Merritt E A and Bacon D J, 1997 Raster3D: Photorealistic molecular graphics. *Methods in Enzymology* **277** 505–524, URL <http://www.bmsc.washington.edu/raster3d/raster3d.html>
- [31] Lindahl E, Hess B and van der Spoel D, 2001 GROMACS 3.0: A package for molecular simulation and trajectory analysis. *J. Mol. Mod.* **7** 306–317, URL <http://www.gromacs.org>
- [32] Hermans J, Berendsen H J C, van Gunsteren W F and Postma J P M, 1984 A consistent empirical potential for water-protein interactions. *Biopolymers* **23** 1513–1518
- [33] Darden T, York D and Pedersen L, 1993 Particle mesh Ewald – an  $N \log(N)$  method for Ewald sums in large systems. *J. Chem. Phys.* **98** 10089–10092
- [34] Berendsen H J C, Postma J P M, DiNola A and Haak J R, 1984 Molecular dynamics with coupling to an external bath. *J. Chem. Phys.* **81** 3684–3690

- [35] Evans R, 1990 Fluids adsorbed in narrow pores: phase equilibria and structure. *J. Phys.: Condens. Matter* **2** 8989–9007
- [36] de Gennes P G, 1985 Wetting: statics and dynamics. *Rev. Mod. Phys.* **57** 827–863
- [37] Unwin N, 2000 The Croonian Lecture 2000. Nicotinic acetylcholine receptor and the structural basis of fast synaptic transmission. *Phil. Trans. Roy. Soc. London B* **355** 1813–1829
- [38] Anishkin A and Sukharev S, 2004 Water dynamics and dewetting transitions in the small mechanosensitive channel MscS, in *Abstracts of the 48th Annual Meeting of the Biophysical Society*, vol. 27-Plat (Biophysical Society)
- [39] Wu Y, Sugimura H, Inoue Y and Takai O, 2002 Thin films with nanotextures for transparent and ultra water-repellent coatings produced from trimethylmethoxysilane by microwave plasma CVD. *Chem. Vapor Depos.* **8** 47–50
- [40] Whitesides G M and Laibinis P E, 1990 Wet chemical approaches to the characterization of organic surfaces: Self-assembled monolayers, wetting, and the physical-organic chemistry of the solid-liquid interface. *Langmuir* **6** 87–96
- [41] Hess B, 1999 *Stochastic concepts in molecular simulation*, Ph.D. thesis, Rijksuniversiteit Groningen, Groningen, URL <http://www.ub.rug.nl/eldoc/dis/science/b.hess/>
- [42] Hautman J and Klein M L, 1991 Microscopic wetting phenomena. *Phys. Rev. Lett.* **67** 1763–1766
- [43] Nijmeijer M J P, Bruin C, Bakker A F and van Leeuwen J M J, 1991 Determination of the location and order of the drying transition with a molecular dynamics simulation. *Phys. Rev. B* **44** 834–837
- [44] Lundgren M, Allan N L, Cosgrove T and George N, 2002 Wetting of water and water/ethanol droplets on a non-polar surface: A molecular dynamics study. *Langmuir* **18** 10462–10466
- [45] Hummer G, Rasaiah J C and Noworyta J P, 2001 Water conduction through the hydrophobic channel of a carbon nanotube. *Nature* **414** 188–190
- [46] Giaya A and Thompson R W, 2002 Water confined in cylindrical micropores. *J. Chem. Phys.* **117** 3464–3475
- [47] Clapham D E, 2003 TRP channels as cellular sensors. *Nature* **426** 517–524
- [48] Beckstein O, Biggin P, Bond P, Bright J, Domene C, Grottesi A, Holyoake J and Sansom M, 2003 Ion channel gating: insights via molecular simulations. *FEBS Lett.* **555** 85–90
- [49] Roosild T P, Miller S, Booth I R and Choe S, 2002 A mechanism of regulating transmembrane potassium flux through a ligand-mediated conformational switch. *Cell* **109** 781–791

- [50] McElroy C, Manfredo A, Wendt A, Gollnick P and Foster M, 2002 TROSY-NMR studies of the 91 kDa TRAP protein reveal allosteric control of a gene regulatory protein by ligand-altered flexibility. *J. Mol. Biol.* **323** 463–473
- [51] Huang X, Margulis C J and Berne B J, 2003 Dewetting-induced collapse of hydrophobic particles. *Proc. Natl. Acad. Sci. USA* **100** 11953–11958
- [52] Adamson A W, 1990 *Physical Chemistry of Surfaces* (John Wiley & Sons, Inc, New York)
- [53] Maibaum L and Chandler D, 2003 A coarse-grained model of water confined in a hydrophobic tube. *J. Phys. Chem. B* **107** 1189–1193
- [54] Harms G S, Orr G, Montal M, Thrall B D, Colson S D and Lu H P, 2003 Probing conformational changes of gramicidin ion channels by single-molecule patch-clamp fluorescence microscopy. *Biophys. J.* **85** 1826–1838